Metrol. Meas. Syst., Vol. 26 (2019) No. 4, pp. 739–755
DOI: 10.24425/mms.2019.129587

METROLOGY AND MEASUREMENT SYSTEMS
Index 330930, ISSN 0860-8229
www.metrology.pg.gda.pl

DEFECT RECOGNITION OF BURIED PIPELINE BASED ON APPROXIMATE ENTROPY AND VARIATIONAL MODE DECOMPOSITION

Haiyang Ju, Xinhua Wang, Tao Zhang, Yizhen Zhao, Zia Ullah

Beijing University of Technology, College of Mechanical Engineering and Applied Electronics Technology, 100 Ping Le Yuan, Chaoyang District, Beijing 100124, China (*haiyoung.ju@gmail.com*, ✉ *juhy2006@gmail.com*, +86 136 9326 4996, *ztao891212@163.com*, *zyzbjut926@163.com*, *engineerziaullah@yahoo.com*)

Abstract

The study aimed to examine the use of Geomagnetic Anomaly Detection (GAD) to locate the buried ferromagnetic pipeline defects without exposing them. However, the accuracy of GAD is limited by the background noise. In the present work, we propose an approximate entropy noise suppression (AENS) method based on Variational Mode Decomposition (VMD) for detection of pipeline defects. The proposed method is capable of reconstructing the magnetic field signals and extracting weak anomaly signals that are submerged in the background noise, which was employed to construct an effective detector of anomalous signals. The internal parameters of VMD were optimized by the Scale–Space algorithm, and their anti-noise performance was compared. The results show that the proposed method can remove the background noise in high-noise background geomagnetic field environments. Experiments were carried out in our laboratory and evaluation results of inspection data were analysed; the feasibility of GAD is validated when used in the application to detection of buried pipeline defects.

Keywords: Buried Pipeline, Defect Recognition, Geomagnetic Anomaly Detection, Variational Mode Decomposition, Approximate Entropy.

1. Introduction

Buried pipelines provide one of the most efficient means of transporting oil and gas, and many countries have attached great importance to the non-destructive testing and safety evaluation of in-service pipelines [1, 2]. After the pipelines were laid and operated, due to the influence of corrosion, third-party damage, natural disasters, and other factors, some defects would inevitably be formed, which requires timely detection of defects through various types of testing methods and evaluation of their impact on pipeline safety. *Non-destructive testing* (NDT) techniques commonly employed in routine pipeline testing are *Ultrasonic Testing* (UT) and *Magnetic Flux Leakage testing* (MFL) [3–6], which are *In-Line Inspection* (ILI) [7]. The ILI should overcome the influence of pipeline running pressure, flow, deformation and pipeline cleanliness on the detection accuracy, whereas the conventional internal detection technology applies only to the

formed macro defects, and it is not effective for stress concentration and early diagnosis of damage in ferromagnetic materials [8, 9].

However, most of the buried pipelines have characteristics that restrict the pigging, so detecting the pipeline defects is an urgent problem to be solved in the non-excavation state. Some external detection techniques currently available include *Eddy Current* (EC) methods [10, 11], *Guided Wave Testing* (GWT) [12–14], *Transient Electromagnetic Method* (TEM) [15], and Radiography. The above means are external electromagnetic excitation detection methods, which increase the difficulty of on-site detection.

The *Metal Magnetic Memory* (MMM) mean [16], which is known as the Magneto-Mechanical Memory method [17], has been employed to close-range ferromagnetic pipeline defect detection by measuring the residual magnetic field [18, 19] above a pipeline. The essence of the residual magnetic field is the external manifestation of stress concentration which leads to an amplification of magnetic field change, and the magnetization effect induced by stress induction cannot establish a corresponding exact formula between the stress and the RMLF [20, 21]. The buried pipelines can be detected using a non-contact magnetic detection technique, where the ILI is difficult to implement [22]. *Magnetic anomaly detection* (MAD) is a good mean for detecting and locating ferromagnetic targets, particularly ferromagnetic buried pipelines [23–27]. The *Magnetic Tomography Method* (MTM) [28, 29] is a passive NDT method, which can detect defects in buried pipelines' bodies by measuring magnetic field anomalies caused by mechanical stress areas of ferromagnetic components. The method can detect defects at the locations far from the pipe and can measure the geometry of the defects.

The leakage magnetic field caused by damage of pipe, however, is affected by various factors such as interference of surrounding magnetic object, signal towers, and high-voltage lines. The non-parametric detection methods have also been studied for MAD, such as high-order crossing method [30] and minimum entropy detector [31]. Since both methods do not need actual assumptions about the target signal, which guarantees them a convenient implementation. However, low *signal-to-noise* (SNR) may assign certain restrains on their detection performance. Therefore, low SNR and the absence of earlier knowledge of the target signal challenge the behavior of MAD. In order to solve the signal processing problem, the *Stochastic Resonance* (SR) algorithm was proposed as a novel detector [32]. However, the method cannot recognize the target signal and the noise signal in passive magnetic detection. The MAD is suitable for detecting magnetic objects of a dipole structure. The detection distance is 2–3 times the maximum size of the magnetic dipole when the detected target can be considered as a point dipole source [22]. Using the magnetic dipole model, Li *et al.* predicted the *Ground Leakage Magnetic Field* (GLMF) above the buried pipeline by simulation [33]. However, it was found that GLMF was lower than the original prediction when changing the pipe material used in the model [34]. The vertical component of the magnetic anomaly signal and its analytic signal were used to detect buried pipelines, which provided an effective method for direction calculating and horizontal locating of buried pipelines [35].

Geomagnetic detection is an effective passive detection method. By measuring the anomaly of the Earth's weak magnetic field, some of their characteristics can be determined in addition to the existence of hidden objects [36]. Soil, water, canopy, and many other types of materials have almost no effect on geomagnetic field. The current challenge in geomagnetic testing is that the detection of weak signals requires expensive instruments. Otherwise, the processing of acquired signals would be very difficult.

We tried to find a more effective mean for GAD to make up for the shortcomings of existing detection methods. This study aimed to examine the use of GAD to locate defects of buried ferromagnetic pipelines without exposing them. An *approximate entropy noise suppression* (AENS)

Metrol. Meas. Syst., Vol. 26 (2019), No. 4, pp. 739–755
DOI: 10.24425/mms.2019.129587

method for geomagnetic anomaly signal detection based on VMD is proposed and applied to ferromagnetic pipeline defect detection. VMD is a new algorithm that decomposes signals into different modes [37], which is an optimized version of the *Empirical Mode Decomposition* (EMD) [38] algorithm for analysing nonlinear and non-stationary signals [39]. The VMD algorithm is successfully used to filter the pipeline defect signal by the de-trended fluctuation analysis [40]. Since the geomagnetic signal is a kind of nonlinear and non-stationary signal, it is critical to study the bandwidth estimation based on the modal instantaneous frequency and instantaneous amplitude spectrum. The VMD can be used to accurately decompose the geomagnetic signal into different modes. In the paper, we propose a novel geomagnetic anomaly detector based on VMD algorithm to improve the detection performance of geomagnetic pipelines. In the actual detection process, the measured magnetic signal can be decomposed into a set of *Intrinsic Mode Functions.* We identified the defect location in a ferromagnetic pipe as GAD, which is considered to be a series of dipole source.

The article is organized as follows. We briefly introduce the optimized VMD algorithm and construct a detector based on VMD in Section 2. The geomagnetic signal is pre-processed by the *Scale–Space* and approximate entropy noise suppression methods. In Section 3, the experiment design is presented. The method of reliability was verified by laboratory experiments and field measurements. Section 4 contains the discussion. Finally, Section 5 concludes the paper.

2. Detector construction based on improved VMD

2.1. Improved VMD algorithm

2.1.1. Basic algorithm of VMD

The VMD is a novel adaptive signal processing algorithm, which assumes that the signal is superimposed by many modal functions. Each modal function is an amplitude modulated and frequency modulated signal with different central frequencies. A variational method is used to minimize the sum of estimated bandwidths of each eigenmode function. The eigenmode functions are demodulated to the corresponding baseband, and finally, the eigenmode functions and corresponding central frequencies are extracted. In the VMD algorithm, the *intrinsic eigenmode function* (IMF) is defined as an Amplitude Modulation-Frequency Modulation signal expressed as:

$$u_k(t) = A_k(t)\cos\left(\phi(t)\right), \tag{1}$$

where: $u_k(t)$ is the modal function; $A_k(t)$ is the instantaneous amplitude of $u_k(t)$; $\phi(t)$ is the instantaneous phase of $u_k(t)$; ω_k is the instantaneous frequency of $u_k(t)$:

$$\omega_k = \phi'(t) = \frac{d\phi(t)}{dt}. \tag{2}$$

The steps should be executed to construct a variational model,

– First, we use Hilbert transform to obtain the analytic signal of each modal function $u_k(t)$, thereby obtaining the unilateral spectrum of the signal.

$$\left[\delta(t) + \frac{j}{\pi t}\right] * u_k(t). \tag{3}$$

– Next, each modal function modulates the spectrum of each eigenmode function to the corresponding baseband by exponential correction around the respective estimated central frequency.

$$\left[\left(\delta(t) + \frac{j}{\pi t}\right) * u_k(t)\right] \mathrm{e}^{-j\omega_k t}. \tag{4}$$

– Finally, the bandwidth of each eigenmode function is estimated by Gaussian smooth demodulation of the signal to obtain the bandwidth of each segment. Thus, the program process is executed by convex optimization problem:

$$\min_{\{u_k\},\{\omega_k\}} \left\{ k \left\| \partial_t \left[\left(\delta(t) + \frac{j}{\pi t} \right) * u_k(t) \right] e^{-j\omega_k t} \right\|_2^2 \right\}, \quad \text{s.t.} \sum_k u_k = x(t), \tag{5}$$

where $\{u_k\} = \{u_1, \ldots, u_K\}$ and $\{\omega_k\} = \{\omega_1, \ldots, \omega_K\}$ are all modes and their central frequencies. $x(t)$ is the input signal. The augmented Lagrangian represented by:

$$\mathcal{L}(u_k(k), \omega_k, \lambda) = \alpha \sum_k \left\| \partial_t \left[\left(\delta(t) + \frac{j}{\pi t} \right) * u_k(t) \right] e^{-j\omega_k t} \right\|_2^2 + \left\| x(t) - \sum_k u_k(t) \right\|_2^2 + \left\langle \lambda(t), x(t) - \sum_k u_k(t) \right\rangle, \tag{6}$$

where: α is a penalty factor, and λ is a Lagrange multiplier. The saddle point is obtained by the Alternate Direction Method of Multipliers. From the Fourier domain solution, all of the obtained central frequencies and modes are updated in the reverse direction. The k-th iteration is updated using:

$$\hat{u}_k^{n+1}(\omega) = \frac{\hat{x}(\omega) - \sum_{i \neq k} \hat{u}_i(\omega) + \frac{\hat{\lambda}(\omega)}{2}}{1 + 2\alpha(\omega - \omega_k)^2}. \tag{7}$$

Wiener filtering is the key part of the VMD algorithm, so it has strong robustness. The update of a central frequency ω_k is at the centre of its corresponding mode power spectrum, which can be given as follows:

$$\omega_k^{n+1} = \frac{\int_0^\infty \omega |\hat{u}_k(\omega)|^2 \, d\omega}{\int_0^\infty |\hat{u}_k(\omega)|^2 \, d\omega}. \tag{8}$$

The focus of this paper is not to show the VMD algorithm in detail. Nevertheless, the paper will delve into the effects of the initial setting of the mode central frequency on the decomposition and the optimal selection of α.

2.1.2. Parameter-less Scale–Space segmentation strategy

In earlier studies, researchers used to estimate the value of K roughly out of their experience, which inevitably brought instability to the results of the analysis. In order to produce a precise calculation, a mathematical method named *Scale–Space* is brought forward to calculate K [41]. In this method, the Fourier spectrum is decomposed into wavelet packets with the ability to accommodate different situations [42]. The paper uses a sampled Gaussian kernel to implement a *Scale–Space* representation:

$$L(x,t) = \sum_{n=-M}^{+M} f(x-n) g(n;t), \tag{9}$$

Metrol. Meas. Syst., Vol. 26 (2019), No. 4, pp. 739–755
DOI: 10.24425/mms.2019.129587

where: the function $f(x)$ is defined in an interval $[0, x_{\max}]$; the kernel function is $g(n;t) = \frac{1}{\sqrt{2\pi t}} e^{-n^2/2t}$; t is a scale parameter. Set $M = C\sqrt{t} + 1$ with $3 \leq C \leq 6$, and with M large enough for the approximate error of the Gaussian to be negligible. $L(x,t)$ is represented by convolution and can preserve detailed information that is longer than $\sqrt{t}$.

By convolution iteration, the different parameter $\sqrt{t}$ determines the spectral segmentation position by detecting all local minimum values of $L(x,t)$. We use a histogram to determine the modes of interest by finding the local minimum that defines a *Scale–Space curve* (SSC). The key issue in finding the modes of interest is the determination of a threshold T of Scale–Space dimension, thereby the SSC of length larger than T is within a mode of interest. At this time, the determination of the threshold is converted into a clustering problem of two types of data on the set L, so we obtain the threshold T using the K-means method that can adaptively divide the Fourier spectrum.

We use a simulation signal to verify the effectiveness of the *Scale–Space* segmentation strategy. The simulation signal consists of four amplitude-modulated signals and random white noise. The corresponding mathematical expressions are as follows:

$$x(t) = x_1(t) + x_2(t) + x_3(t) + x_4(t) + x_{noise}, \tag{10}$$

$$\begin{aligned} x_1(t) &= \cos(100\pi t), \\ x_2(t) &= 3e^{-4t}\cos(300\pi t), \\ x_3(t) &= \sin(\cos(500\pi t)), \\ x_4(t) &= 0.5\cos(800\pi t). \end{aligned} \tag{11}$$

The signal spectrum is shown in Fig. 1. Obviously, the signals of different frequencies can be accurately divided, as shown in Fig. 1a. Furthermore, we use the scale–space method to optimize VMD for calculation, as shown in Fig. 1b. The spectrum of signal components obtained by VMD is consistent with each input signal. The simulation results show that the performance of VMD algorithm can be effectively improved by using the Scale–Space segmentation strategy.

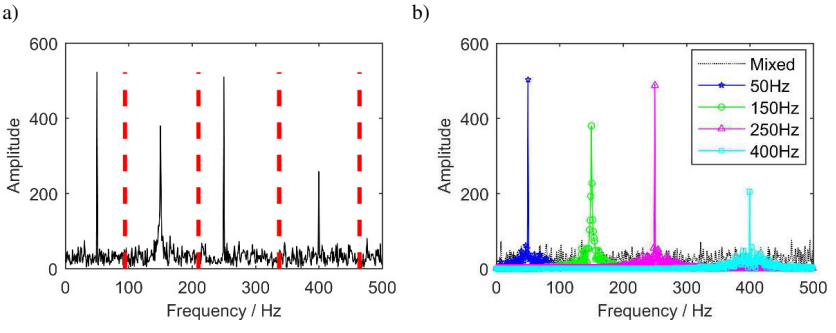

Fig. 1. Analysis of *Signal Spectrum* using the *Scale–Space Segmentation Strategy*. a) Segmentation results obtained with the scale–space method; b) signal spectra based on the scale–space and VMD.

2.1.3. Approximate entropy noise suppression

Approximate entropy (ApEn) is a measure that quantifies the predictability or regularity of a time series data [43]. ApEn considers a time sequence of points in a time series, so it is the

preferred measure of randomness or regularity. A given time series is $\{x(i),\ i = 1, 2, \ldots, N\}$. Next, we define for each i:

$$C_i^m(r) = \frac{1}{N-m+1} \sum_{j=1} \theta\left(r - d\left(x(i),\ x(j)\right)\right), \tag{12}$$

where m and r are the values of mode dimension and the vector comparison distance, respectively. $\theta(x) = 1$ for $x > 0$, $\theta(x) = 0$; otherwise, it represents standard Heavyside function, and is the maximum distance between any two modes.

Then, we define $\phi^m(r)$ as:

$$\phi^m(r) = \frac{1}{N-m+1} \sum_{i=1}^{N-m+1} \log C_i^m(r). \tag{13}$$

Finally, the ApEn is:

$$\mathrm{ApEn}(m, r) = \phi^m(r) - \phi^m(r+1). \tag{14}$$

ApEn is a dimensionless scalar, whose magnitude depends on m and r. Therefore, the paper proposed a method of extracting the "noise-suppressed" feature of the geomagnetic signal by combining the correlation function and ApEn theory, *i.e.*, *Approximate Entropy Noise Suppression* (AENS). The specific feature extraction process is as follows:

- First, the autocorrelation function of the geomagnetic signal is calculated. The correlation function value is taken as the calculation sequence of ApEn, and the sequence length of the geomagnetic signal used in ApEn is longer than that of the correlation signal.
- Finally, the ApEn of the selected function is calculated to obtain the measurement of signal complexity.

We calculated the ApEn of the autocorrelation function of geomagnetic signals from the experimental data. The data of pipeline defect signals used for calculation contain 100,000 sampling points, as shown in Fig. 2a. When calculating the ApEn, the sample data are divided into 100 segments, and each segment has 1000 sampling points corresponding to an ApEn of the autocorrelation function. The results show that the ApEn of geomagnetic signals is between 0.43 and 0.55, as shown in Fig. 2b.

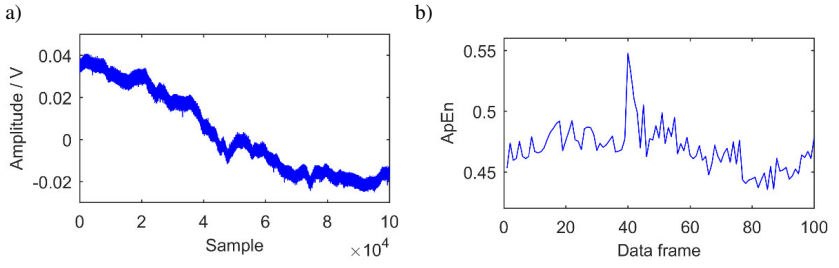

Fig. 2. A sample geomagnetic signal and ApEn of the autocorrelation function. a) The geomagnetic detection signal for pipeline defects; b) the ApEn of autocorrelation function value of the geomagnetic signal.

2.2. Geomagnetic anomaly detection model

It is difficult to extract target signal under the condition of low SNR. However, the traditional signal processing means are based on the assumption that both the signal to be measured and the noise signal are sampled at the same time. The sampled signal is directly de-noised, and the

Metrol. Meas. Syst., Vol. 26 (2019), No. 4, pp. 739–755
DOI: 10.24425/mms.2019.129587

eigenvalues are extracted. The de-noising process needs a long time to fit the strong noise, and the results occasionally have unacceptable errors. Therefore, extracting a weak geomagnetic anomaly signal is the key to detect pipeline damage under strong background geomagnetic interference. The geomagnetic anomaly detection model based on VMD is presented in Fig. 3. The algorithm flowchart is as follows:

- the target signal is pre-processed by the Scale–Space segmentation, and the mode number K used in VMD is determined;
- calculate the correlation coefficient between the geomagnetic anomaly signalbased on the approximate entropy value and the original signal, and determine the value of constraint parameter α;
- construct pipeline defect geomagnetic anomaly signal detector based on VMD;
- use VMD detector to de-noise and reconstruct signals.
- assess whether the result satisfies the *Scale–Space* segmentation and approximate entropy de-noising algorithm or not;
- finally, if the result does not meet the requirements, repeat steps 1–4 to complete the entire de-noising process; if it is satisfactory, the reconstructed signal is recorded as the final de-noising result.

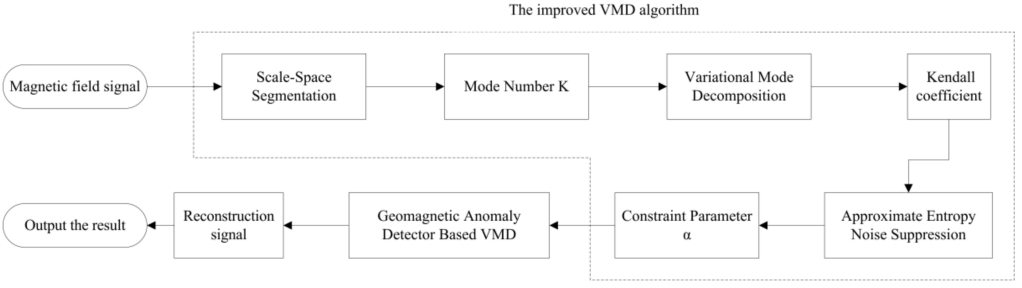

Fig. 3. A flowchart of the *Geomagnetic Anomaly Detector Construction* based on the improved VMD algorithm.

3. Results and analysis

3.1. VMD algorithm analysis

The VMD algorithm is applied to analyse subtlechanges of magnetic anomaly signals. The correctness of the results will be affected by the selection of VMD input parameters. Therefore, this section discusses the selection of values of two key parameters, *i.e.*, the mode number K and the constraint constraint α. The VMD algorithm can only perform well when the balancing parameter of α and the mode number K are properly set.

3.1.1. Number of mode components K

The Scale–Space algorithm is applied to geomagnetic anomaly signals, and the spectrum of signals is divided into seventeen segments, as shown in Fig. 4a. Therefore, the number K is set to seventeen. It is noteworthy that the larger K will bring trouble to the calculation, so the number of modes should be reduced.

The spectrum analysis on pipeline defect signal shows that the signal energy concentrates mostly within the band of smaller than 5 Hz. Concerning this fact, the defect signal is identified

into four modal components in order to obtain a certain signal, as shown in Fig. 4b. The energy outside 5 Hz can be considered as 0. In conclusion, a band-pass filter designed to the pass signals only smaller than 5 Hz is chosen, and the number of mode components K is set to 4.

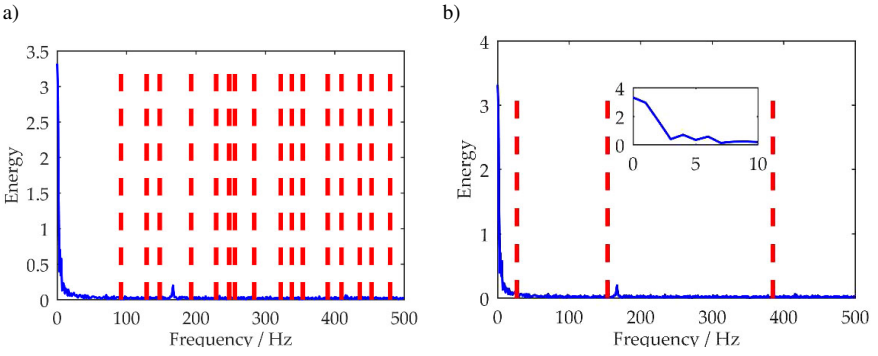

Fig. 4. Segmentation results obtained with the scale–space method. a) Seventeen modes; b) four modes.

3.1.2. Constraint parameter α

The problem that the balance constraint parameters cannot be given accurately in the process of variational mode decomposition is discussed, *i.e.*, the bandwidth of signal mode component is inversely proportional to the value of α. As the balance constraint parameter decreases, the bandwidth of each mode component increases; thus, the phenomenon of central frequency overlapping and mode aliasing is apt to occur. With bigger α the mode bandwidth will be narrower. Therefore, the anti-noise performance of the VMD algorithm will be improved, but the amount of calculation will increase.

As to the GAD in this paper, it depends largely on whether the central frequency of the extracted mode component is correct or not, so it is important to select a balance point of α. The experimental data were used to analyse the anti-noise performance at different α values, so as to select an appropriate value of α. It has been generally recognized that when α exceeds 5000, the numerical error in mode separation would be too large to ignore [44]. Therefore, the scope of α is limited by [100, 5000]. The calculation is carried out in ascending order of α from 100 to 5000 at the pace of 100, some results of calculation are chosen to list here when α is at key values. It must be pointed out that, in Figs. 5c–5e, when α is larger than 2500, the CFs of noise are almost the same as the original signals, which indicated good anti-noise performance. However, α larger than 2500 cannot be of being employed because the reconstructed signal deviates seriously from the true value.

Furthermore, the *Approximate Entropy* (ApEn) and *Kendall coefficients* (KCs) are used as the criteria to measure the effect of signal filtering. ApEn is a measure of the signal volatility after filtering, and KC is a measure of the correlation between the reconstructed signal and the original signal. The quality of the reconstructed signal is directly proportional to KC and inversely to ApEn. Fig. 6. shows that both ApEn and KC decrease gradually when the value of α is between 100 and 5000. The ApEn is greater than 0.55 (The value is calculated in 2.1.3) for values of α from within the range of 100–1500, which should be discarded.

Therefore, the value of constraint parameter α should be set to 2000 to ensure the correct value of central frequency, as shown in Table 1.

Metrol. Meas. Syst., Vol. 26 (2019), No. 4, pp. 739–755
DOI: 10.24425/mms.2019.129587

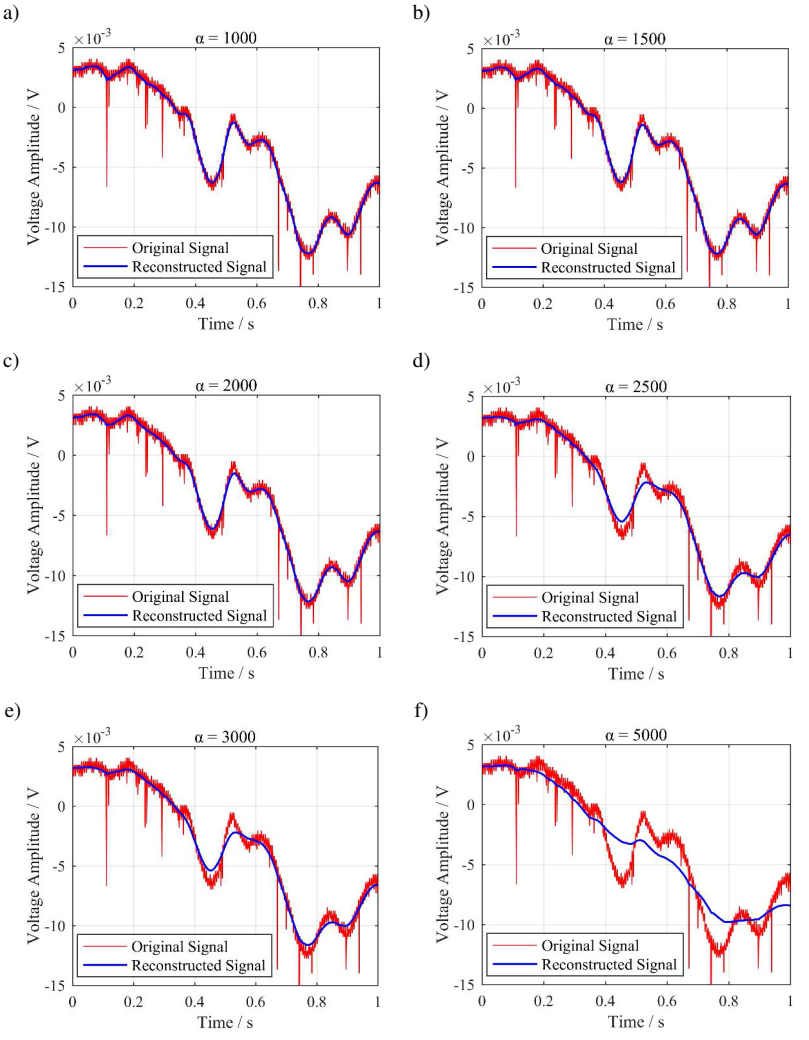

Fig. 5. The original signal and the signal reconstructed at different values of α. a) α = 1000; b) α = 1500; c) α = 2000; d) α = 2500; e) α = 3000; f) α = 5000.

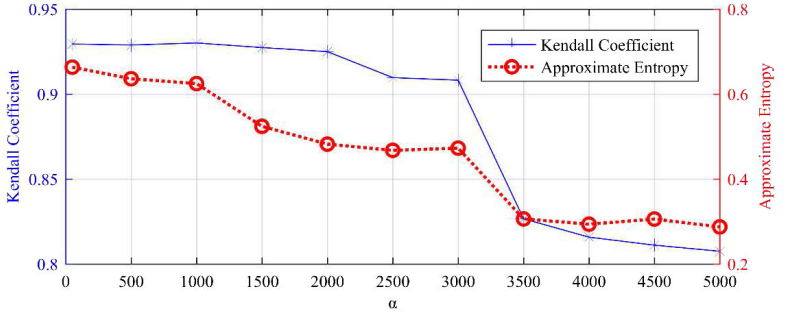

Fig. 6. Variation of *Kendall Coefficient* and *Approximate Entropy* with the value of α. The left vertical axis presents Kendall coefficient values, whereas the right one – *Approximate Entropy* values.

Table 1. The variation trend of *Kendall Coefficient* and *Approximate Entropy* values with values of α.

Index	**1**	**2**	**3**	**4**	**5**	**6**	**7**	**8**	**9**	**10**	**11**
Value of α	50	500	1000	1500	2000[1]	2500	3000	3500	4000	4500	5000
Kendall Coefficient	0.930	0.929	0.930	0.927	0.925	0.910	0.908	0.827	0.816	0.811	0.808
Approximate Entropy	0.663	0.636	0.625	0.524	0.482	0.468	0.473	0.306	0.294	0.306	0.287

[1] The appropriate value of α for geomagnetic signals.

3.2. Experimental results

3.2.1. Experimental data

Firstly, a simplified geomagnetic anomaly detection model for buried pipeline defects is established, as shown in Fig. 7a. The experimental system consists of a sensor array, a module of data acquisition, a module of signal conditioning and power supply, a satellite positioning system, as shown in Fig. 7b.

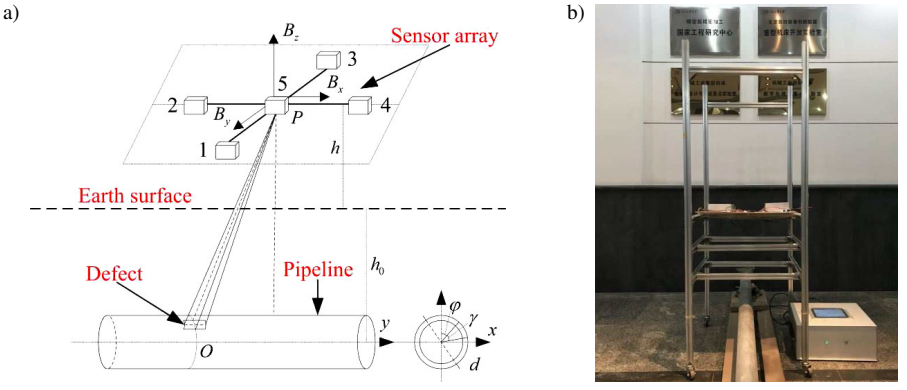

Fig. 7. The laboratory experiment of pipeline inspection. a) A schematic diagram of the experimental setup; b) the experimental system.

The experimental pipe is made of Q235 steel material with a wall thickness of 3 mm, and a diameter of 75 mm. We fabricated six defects at different locations of the pipe to study the magnetic anomaly signals of different defects, as shown in Fig. 8.

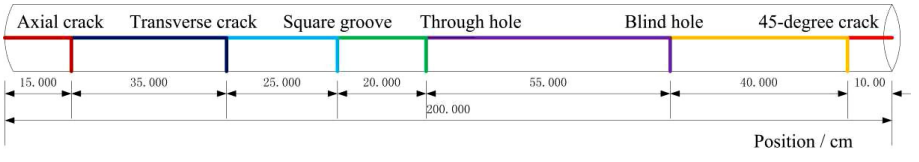

Fig. 8. Locations of defects in the pipeline.

The shapes of these six defects are axial crack, transverse crack, square groove, through hole, blind hole, and 45-degree crack in turn, as shown in Fig. 9. The lift-off is five times the pipeline diameter.

Metrol. Meas. Syst., Vol. 26 (2019), No. 4, pp. 739–755
DOI: 10.24425/mms.2019.129587

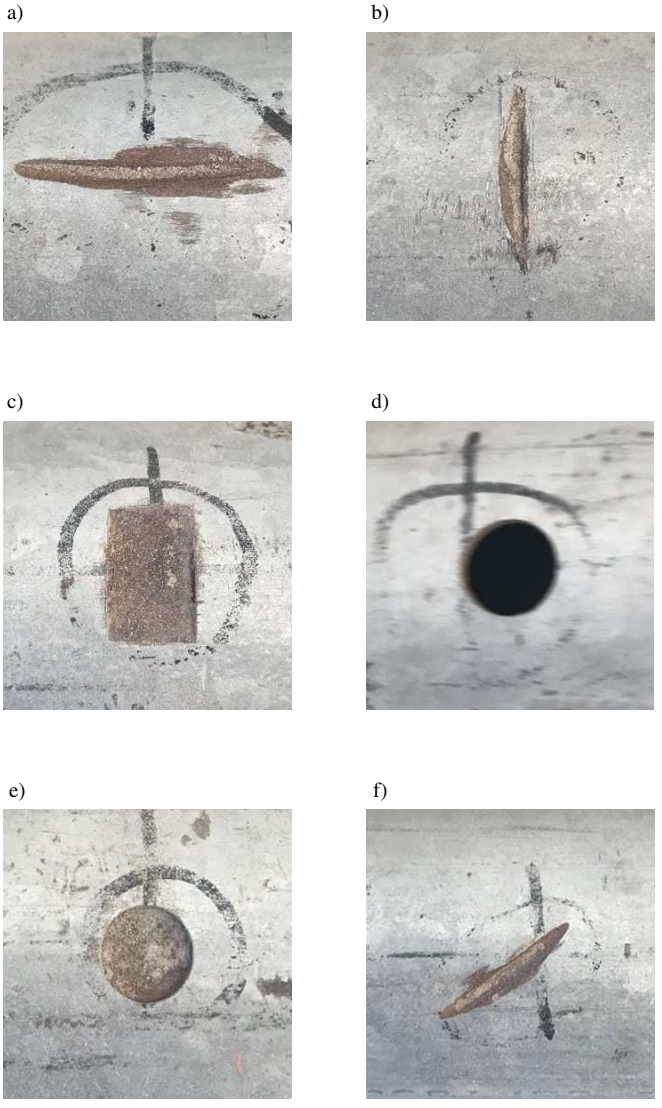

Fig. 9. Images of defects in the ferromagnetic pipeline. a) The size of the axial crack is 30 mm × 1 mm × 1 mm; b) The size of the axial crack is 1 mm × 20 mm × 1 mm; c) the size of the axial crack is 12 mm × 20 mm × 1 mm; d) the diameter of the through hole is 10mm; e) the diameter and depth of the blind hole are 10 mm and 1 mm; f) the size of the 45-degree crack is 1 mm × 20 mm × 1 mm.

The experimental data used inthe paper consist of two different data sets, as shown in Fig. 10a and Fig. 11a. The first set of signals contains the experimental data detected without artificial excitation interference, so that we can obtain a high-SNR signal. The testing conditions simulate the real field environment. The second group of signals are the test data after adding a 1 kHz interference signal artificially to obtain a low-SNR signal. In order to save the analysis space, the second set of data analysed only 0–100 cm signals. We analysed the second group of signals, which verified the effectiveness of the APNS algorithm.

3.2.2. Results of data analysis

Figures 10a, 10b present the original pipeline defect signal and gradient energy index, respectively. Based on these two figures, the defect location and damage degree on the pipeline cannot be identified. Therefore, we process the original signal using VMD and the gradient energy detector. Fig. 10c shows the component of geomagnetic anomaly signal extracted by VMD. We use the VMD detector to perform *Energy Index* processing on the signal, and locations of six defect signals can be seen very clearly on the pipeline, as shown in Fig. 10d.

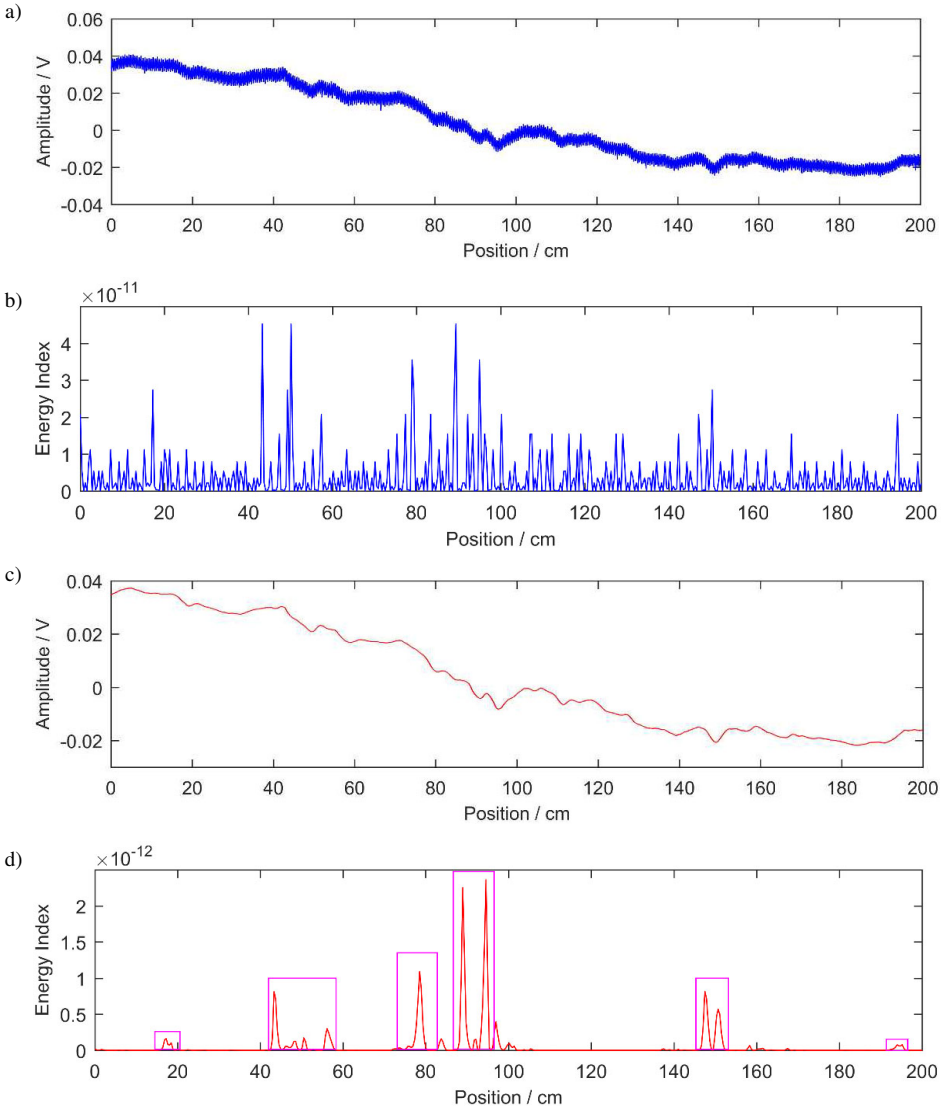

Fig. 10. Detection of defects in a buried ferromagnetic pipeline in the geomagnetic environment. a) The original detection signal of a pipeline defect; b) A pipeline defect signal processed by the gradient energy detector; c) The component of geomagnetic anomaly signal extracted by the VMD detector; d) Corresponding positions of six defects in the pipeline.

Metrol. Meas. Syst., Vol. 26 (2019), No. 4, pp. 739–755
DOI: 10.24425/mms.2019.129587

Table 2 shows the actual and calculated locations of pipeline defects. The results show that the relative error is less than 2% for the pipeline with a length of 200 cm.

Table 2. Error analysis of pipeline defect locations.

Defect Type	Axial Crack	Transverse Crack	Square Groove	Through Hole	Blind Hole	45-Degreek Crack
Actual Position / cm	15	50	75	95	150	190
Calculated Interval Position / cm	17–19	43–57	75–80	88–96	147–152	192–196
Calculated Midpoint Position / cm	18.0	50.0	77.5	92	149.5	194
Absolute Error / cm	3.0	0.0	2.5	3	0.5	4
Relative Error / %	1.50	0	1.25	1.50	0.25	2.00

In the second experiment, we added 1 kHz Gauss noise to acquire low-SNR signals. Fig. 11 shows the first half length of the pipeline, *i.e.*, 0–100 cm. Fig. 11a describes the signal obtained by the magnetic sensor, in which the signal is practically hidden in artificially added noise. The location of pipeline defect and the degree of damage cannot be identified without the VMD detector, as shown in Fig. 11c. Therefore, we have input the signal with noise to the VMD detector (Fig. 11b), and the output signal, *i.e.*, *Energy Index*, is shown in Fig. 11d. The pipeline defect can be represented at the output of VMD detector, which proves the effectiveness of the VMD detector. It is estimated that the SNR of signal after filtered by VMD detector is approximately eight times that of the input (here, we define the SNR as a ratio of signal amplitude to noise amplitude), which also indicated that the effectiveness of detection.

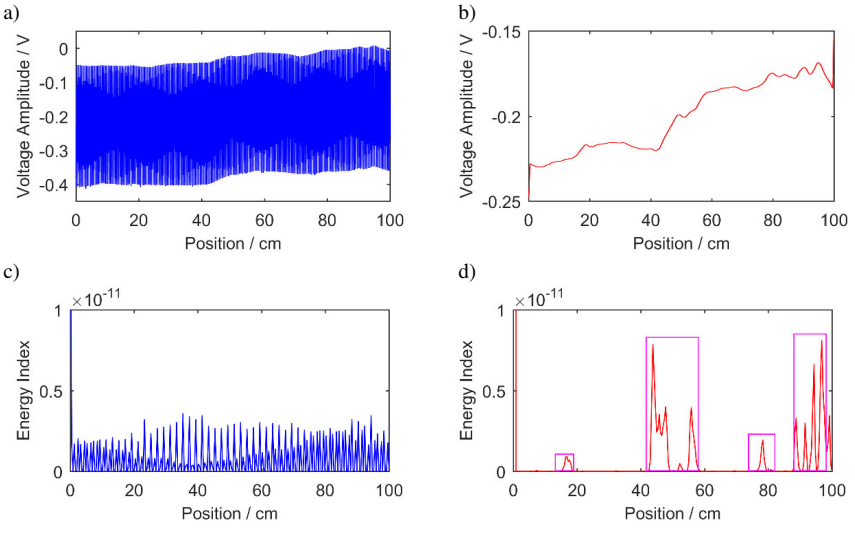

Fig. 11. Detection of defects in a buried ferromagnetic pipeline after adding noise. a) The original detection signal of a pipeline defect; b) the component of geomagnetic anomaly signal extracted by the VMD detector; c) t pipeline defect signal processed by the gradient energy detector; d) corresponding positions of four defects in the pipeline.

Table 3 shows the actual and calculated locations of pipeline defects. The results show that the relative error is less than 2% for the pipeline with a length of 100 cm.

Table 3. Error analysis of pipeline defect locations.

Defect Type	Axial Crack	Transverse Crack	Square Groove	Through Hole
Actual Postion / cm	15	50	75	95
Calculated Interval Position /cm	16–19	41–58	78–80	88–99
Calculated Midpoint Position /cm	17.5	49.5	79.0	93.5
Absolute Error / cm	2.5	0.5	4.0	1.5
Relative Error / %	1.25	0.03	2.00	0.75

4. Discussion

By observing the original experimental data of the first and second sets, we cannot directly determine the pipeline damage degree and its corresponding location from the original data. The first experiment shows that a pipeline defect signal is detected in the geomagnetic environment. Although signal fluctuations can be observed from the first set of raw data, we still cannot identify pipeline defects. In the second group of experiments, a pipeline defect signal was completely submerged in artificially added noise. To further describe the performance of VMD detector, we transform the original signal into a *receiver operating characteristic* (ROC) curve. Therefore, we can reconstruct target signals for magnetic field signals of any pipeline direction, magnetic moment direction, and any signal-to-noise ratio value. The future research can include testing the performance of the proposed detector, *i.e.*, using synthetic target signals and acquired magnetic noise to obtain ROC curves.

The OBF detector and its modified model proposed in [45] are greatly influenced by the shape of the target signal, while the VMD detector is immune to that effect and can provide an adaptive approximation testing for a class of abnormal signals. The reason is that the VMD detector is not designed according to the specific features of the detected magnetic signal. However, the initial parameters of VMD detector proposed in this paper can be optimized to accommodate various types of abnormal signals, such as peak and pass-band signals. In the future work, we will concentrate effort on making VMD detectors more suitable for magnetic anomaly signals of any shape.

5. Conclusions

In the article, a novel feature signal extraction algorithm based on improved VMD is proposed for GAD of defects in a buried ferromagnetic pipeline. We have applied VMD to calculate the z-axis component of the pipeline's magnetic signal measured by a total-field magnetic sensor along a direction of straight track in the geomagnetic background. The VMD results in obtaining the geomagnetic anomaly signal component, which is then employed as GAD to construct an "energy" detector. This method is not only convenient to extract the time-frequency characteristics of magnetic anomaly signals but also conducive to the coupling analysis of magnetic field signals between different frequency bands. The results of applying VMD-GAD in the experiments showed that the peak of the coupling strength appeared when the frequency band was narrower than 5 Hz, and pipeline defects could be located by using a specified frequency band signal with an error not exceeding 2%. While the measured signal is submerged in the environment, the output signal

Metrol. Meas. Syst., Vol. 26 (2019), No. 4, pp. 739–755
DOI: 10.24425/mms.2019.129587

of the VMD detector is visible. The high detection accuracy and low computational complexity make the proposed detector attractive for detection of defects in buried ferromagnetic pipelines.

Acknowledgements

This work is supported by the National Key Research and Development Program of China (project number: 2017YFC0805005-1), the Collaborative Innovation Project of Chaoyang District Beijing China (project number: CYXC1709), and the Science and Technology Program of Beijing Municipal Education Commission (project number: KZ201810005009).

References

[1] Li, Z., Jarvis, R., Nagy, P.B., Dixon, S., Cawley, P. (2017). Experimental and simulation methods to study the Magnetic Tomography Method (MTM) for pipe defect detection. *NDT&E Int.*, 92, 59–66.

[2] Xu, X., Liu, M., Zhang, Z., Jia, Y. (2014). A Novel High Sensitivity Sensor for Remote Field Eddy Current Non-Destructive Testing Based on Orthogonal Magnetic Field. *Sensors*, 14(12), 24098–24115.

[3] Vanaei, H.R., Eslami, A., Egbewande, A. (2017). A review on pipeline corrosion, in-line inspection (ILI), and corrosion growth rate models. *International Journal of Pressure Vessels and Piping*, 149, 43–54.

[4] Quarini, J., Shire, S. (2007). A Review of Fluid-Driven Pipeline Pigs and their Applications. *Proc. Inst. Mech. Eng., Part E*, 221(1), 1–10.

[5] Karami, M. (2012). Review of Corrosion Role in Gas Pipeline and Some Methods for Preventing It. *J. Pressure Vessel Technol.*, 134(5), 054501.

[6] Pan, S., Xu, Z., Li, D., Lu, D. (2018). Research on Detection and Location of Fluid-Filled Pipeline Leakage Based on Acoustic Emission Technology. *Sensors*, 18(11), 3628.

[7] Feng, Q., Li, R., Nie, B., Liu, S., Zhao, L., Zhang, H. (2016). Literature Review: Theory and Application of In-Line Inspection Technologies for Oil and Gas Pipeline Girth Weld Defection. *Sensors*, 17(12), 50.

[8] Liu, B., He, L., Zhang, H., Cao, Y., Fernandes, H. (2017). The axial crack testing model for long distance oil-gas pipeline based on magnetic flux leakage internal inspection method. *Measurement*, 103, 275–282.

[9] Layouni, M., Hamdi, M.S., Tahar, S. (2017). Detection and sizing of metal-loss defects in oil and gas pipelines using pattern-adapted wavelets and machine learning. *Appl Soft Comput.*, 52, 247–261.

[10] Li, Y., Yan, B., Li, D., Li, Y., Zhou, D. (2016). Gradient-field pulsed eddy current probes for imaging of hidden corrosion in conductive structures. *Sens. Actuators, A*, 238, 251–265.

[11] Feng, B., Ribeiro, A., Rocha, T., Ramos, H. (2018). Comparison of Inspecting Non-Ferromagnetic and Ferromagnetic Metals Using Velocity Induced Eddy Current Probe. *Sensors*, 18(10), 3199.

[12] Lowe, M.J.S., Alleyne, D.N., Cawley, P. (1998). Defect detection in pipes using guided waves. *Ultrasonics*, 36(1–5), 147–154.

[13] Alleyne, D.N., Pavlakovic, B., Lowe, M.J.S., Cawley, P. (2004). Rapid, Long Range Inspection of Chemical Plant Pipework Using Guided Waves. *Key Eng. Mater.*, 270–273, 434–441.

[14] Honarvar, F., Salehi, F., Safavi, V., Mokhtari, A., Sinclair, A.N. (2013). Ultrasonic monitoring of erosion/corrosion thinning rates in industrial piping systems. *Ultrasonics*, 53(7), 1251–1258.

[15] Hu, B., Yu, R., Liu, J. (2016). Experimental study on the corrosion testing of a buried metal pipeline by transient electromagnetic method. *Anti-Corros. Methods Mater.*, 63(4), 262–268.

[16] Dubov, A.A. (1997). A study of metal properties using the method of magnetic memory. *Met. Sci. Heat Treat.*, 39(9), 401–405.

[17] Jiles, D.C. (1999). Theory of the magnetomechanical effect. *J. Phys. D. Appl. Phys.*, 32(15), 1945–1945.

[18] Dubov, A., Kolokolnikov, S. (2013). The metal magnetic memory method application for online monitoring of damage development in steel pipes and welded joints specimens. *Weld. World*, 57(1), 123–136.

[19] Lin, S., Wang, W., Zhao, C., Feng, Z., Bi, W., Jiang, X. (2011). Application of Metal Magnetic Memory Method in Long-Distance Oil and Gas Pipeline Defects Detection. *ICPTT*.

[20] Hu, B., Li, L., Chen, X., Zhong, L. (2010). Study on the influencing factors of magnetic memory method. *Int J Appl Electrom.*, 33(3–4), 1351–1357.

[21] Augustyniak, M., Usarek, Z. (2015). Discussion of Derivability of Local Residual Stress Level from Magnetic Stray Field Measurement. *J. Nondestruct Eval.*, 34(3).

[22] Sheinker, A., Moldwin, M.B. (2016). Magnetic anomaly detection (MAD) of ferromagnetic pipelines using principal component analysis (PCA). *Meas. Sci. Technol.*, 27(4), 045104.

[23] Liu, Z., Pang, H., Pan, M., Wan, C. (2016). Calibration and Compensation of Geomagnetic Vector Measurement System and Improvement of Magnetic Anomaly Detection. *IEEE Geosci Remote S.*, 1–5.

[24] Birsan, M. (2011). Recursive Bayesian Method for Magnetic Dipole Tracking With a Tensor Gradiometer. *IEEE Trans. Magn.*, 47(2), 409–415.

[25] Zalevsky, Z., Bregman, Y., Salomonski, N., Zafrir, H. (2012). Resolution Enhanced Magnetic Sensing System for Wide Coverage Real Time UXO Detection. *J. Appl. Geophys.*, 84, 70–76.

[26] Eppelbaum, L.V. (2011). Study of magnetic anomalies over archaeological targets in urban environments. *Phys. Chem. Earth. Parts A/B/C*, 36(16), 1318–1330.

[27] Sheinker, A., Frumkis, L., Ginzburg, B., Salomonski, N., Kaplan, B.-Z. (2009). Magnetic Anomaly Detection Using a Three-Axis Magnetometer. *IEEE Trans. Magn.*, 45(1), 160–167.

[28] Liao, K., Yao, Q., Zhang, C. (2011). Principle and Technical Characteristics of Non-Contact Magnetic Tomography Method Inspection for Oil and Gas Pipeline. *ICPTT*, 2011.

[29] Kolesnikov, I. (2014). Magnetic Tomography Method (MTM) &ndash A Remote Non-destructive Inspection Technology for Buried and Sub Sea Pipelines. *OTC Arctic Technology Conference*.

[30] Sheinker, A., Ginzburg, B., Salomonski, N., Dickstein, P.A., Frumkis, L., Kaplan, B.-Z. (2012). Magnetic Anomaly Detection Using High-Order Crossing Method. *IEEE T Geosci. Remote*, 50(4), 1095–1103.

[31] Sheinker, A., Salomonski, N., Ginzburg, B., Frumkis, L., Kaplan, B.-Z. (2008). Magnetic anomaly detection using entropy filter. *Meas. Sci. Technol.*, 19(4), 045205.

[32] Wan, C., Pan, M., Zhang, Q., Wu, F., Pan, L., Sun, X. (2018). Magnetic anomaly detection based on stochastic resonance. *Sens. Actuators, A*, 278, 11–17.

[33] Li, C., Chen, C., Liao, K. (2015). A quantitative study of signal characteristics of non-contact pipeline magnetic testing. *Insight – Non-Destructive Testing and Condition Monitoring*, 57(6), 324–330.

[34] Jarvis, R., Cawley, P., Nagy, P. B. (2017). Performance evaluation of a magnetic field measurement NDE technique using a model assisted Probability of Detection framework. *NDT&E Int.*, 91, 61–70.

[35] Guo, Z., Liu, D., Pan, Q., Zhang, Y., Li, Y., Wang, Z. (2015). Vertical magnetic field and its analytic signal applicability in oil field underground pipeline detection. *J. Geophys. Eng.*, 12(3), 340–350.

[36] Hirota, M., Furuse, T., Ebana, K., Kubo, H., Tsushima, K., Inaba, T., Shima, A., Fujinuma, M., Tojyo, N. (2001). Magnetic detection of a surface ship by an airborne LTS SQUID MAD. *IEEE Trans. Appl. Supercon.*, 11(1), 884–887.

[37] Dragomiretskiy, K., Zosso, D. (2014). Variational Mode Decomposition. *IEEE Trans. Signal Proces.*, 62(3), 531–544.

[38] Huang, N.E., Shen, Z., Long, S.R., Wu, M.C., Shih, H.H., Zheng, Q., Yen, N.-C., Tung, C.C., Liu, H.H. (1998). The empirical mode decomposition and the Hilbert spectrum for nonlinear and non-stationary time series analysis. *Proc. R. Soc. London, Ser. A*, 454(1971), 903–995.

[39] Mert, A. (2016). ECG feature extraction based on the bandwidth properties of variational mode decomposition. *Physiol. Meas.*, 37(4), 530–543.

[40] Ma, W., Yin, S., Jiang, C., Zhang, Y. (2017). Variational mode decomposition denoising combined with the Hausdorff distance. *Rev. Sci. Instrum.*, 88(3), 035109.

[41] Gao, Z., Wang, X., Lin, J., Liao, Y. (2017). Online evaluation of metal burn degrees based on acoustic emission and variational mode decomposition. *Measurement*, 103, 302–310.

[42] Gilles, J., Heal, K. (2014). A parameterless scale–space approach to find meaningful modes in histograms – Application to image and spectrum segmentation. *Int. J. Wavelets Multi.*, 12(06), 1450044.

[43] Ocak, H. (2009). Automatic detection of epileptic seizures in EEG using discrete wavelet transform and approximate entropy. *Expert. Syst. Appl.*, 36(2), 2027–2036.

[44] Wang, Y., Markert, R. (2016). Filter bank property of variational mode decomposition and its applications. *Signal Process.*, 120, 509–521.

[45] Sheinker, A., Shkalim, A., Salomonski, N., Ginzburg, B., Frumkis, L., Kaplan, B.-Z. (2007). Processing of a scalar magnetometer signal contaminated by $1/f\alpha$ noise. *Sens. Actuators, A*, 138(1), 105–111.